Parallel Blade-Vortex Interactions: An Experimental Study and Comparison with Computations

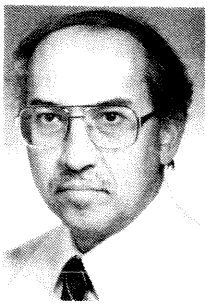

C. Kitaplioglu
Aerospace Engineer
Rotorcraft Aeromechanics Branch

F. X. Caradonna
Staff Scientist, U.S. Army ATCOM
Aeroflightdynamics Directorate

C.L. Burley
Research Engineer
Acoustics Division
NASA Langley Research Center
Hampton, Virginia

NASA Ames Research Center
Moffett Field, California

This paper presents results from an experimental study of rotor blade-vortex interaction (BVI) aerodynamics and acoustics. The experiment utilized an externally generated vortex interacting with a two-bladed rotor operating at zero thrust to minimize the influence of the rotor's own wake. The rotor blades were instrumented with a total of 60 absolute pressure transducers at three spanwise and ten chordwise stations on both the upper and lower surfaces. Acoustic data were obtained with fixed near-field microphones as well as a movable array of far-field microphones. The test was carried out in the acoustically treated test section of the NASA Ames 80- by 120-Foot Wind Tunnel. Several parameters which influence BVI, such as vortex-rotor separation distance, vortex strength, and vortex sense (swirl direction), as well as rotor tip Mach number and advance ratio, were varied. Simultaneous measurements were obtained of blade surface pressure distributions, near-field acoustics, and far-field acoustics during the vortex-blade encounters. A comparison with computational results from the WOPWOP code shows good correlation with experimental data.

Nomenclature

c	blade chord
c_{vg}	vortex generator wing chord
$C_p = (p - p_s)/0.5*\rho*V_\infty^2$	pressure coefficient
$L_p = 20 \log_{10}(p/p_{ref})$	Sound Pressure Level (dB)
M_{tip}	hover tip Mach number
p	pressure
p_{ref}	reference pressure (2×10^{-5} Pascals, unless otherwise noted)
p_s	static pressure
r	blade spanwise coordinate
R	rotor radius
$V_\infty = \Omega R\ (\mu + r/R \cos\psi)$	local free stream velocity
x, y, z	coordinate system centered on the rotor hub
z_v	vortex location relative to rotor plane
α_v	vortex generator angle of attack
χ_{bvi}	BVI pressure increment
ϕ	elevation angle measured positive down from rotor plane
Γ_v	vortex circulation
μ	rotor advance ratio
Π_{bvi}	BVI acoustic amplitude
ρ	density
Ω	rotor rotational speed (rad/sec)
ψ	azimuth angle measured positive in direction of rotation; ψ=0 downstream
ζ_v	core size (ratio of maximum tangential velocity radius / vortex generator chord)

Presented at the American Helicopter Society 2nd International Aeromechanics Specialists' Conference, Bridgeport, CT, October 11-13, 1995. Manuscript received May 1996; accepted Feb. 1997.

Introduction

The interaction of a rotor with one or more of its tip vortices can occur in many forms and is a topic of considerable interest. Such interactions are a primary source of rotor vibratory loading. When the rotor blade and the tip vortex are very close and nearly parallel to each other, the interaction is particularly strong (though of short duration) and is a major source of rotorcraft noise. This type of interaction is usually referred to as a parallel "BVI" (Blade-Vortex Interaction) and is the subject of this experimental investigation.

A large number of aerodynamic and acoustic computational codes (Refs. 1-5), embodying a wide range of physical models of BVI, have been developed. The aerodynamic models range from two-dimensional, ideal-flow, "vortex-cloud" methods employing conformal mapping solutions to 3-D, compressible Euler/Navier-Stokes CFD methods — with the middle-ground being held by 3-D full-potential CFD methods. Acoustic prediction methods are of two types; the acoustic analogy methods and the more recent Kirchhoff methods. CFD is also used for acoustics but cannot practically be extended to the far-field that acoustics is ultimately concerned with. Nevertheless, CFD has great potential for providing input for Kirchhoff methods. The choice between these methods is dependent on the extent to which flow-field non-linearity dominates the solution. Therefore the near-field aerodynamics is of critical importance both for determining the essential physics and the type of acoustic method that must be used. Developing combined aeroacoustic computational methods in which we have high confidence is crucially important. Such confidence requires validation using the simplest possible tests. Until the present, however, most BVI aeroacoustic tests have involved the use of rotor models operating at typical flight conditions. The complexities of typical rotor flows (with wake geometries whose strength and locations with respect to the blade are difficult to determine) are considerable. Here a different approach was taken by performing an experiment which, rather than operating a rotor under typical flight conditions generating BVI, creates a situa-

tion that closely resembles the simplified geometry found in the most basic CFD codes. In effect, rather than refining the model to account for real world complexities, we have attempted to refine the experiment to reflect the simplest possible computational model of BVI. If the codes cannot do a good job of correlating with a simplified experiment, there is little reason to expect good correlation with real flight data with all of its complications.

This paper describes the wind tunnel experiment designed to investigate the fundamentals of BVI aeroacoustics and presents some representative blade pressure and far-field acoustic data. Also, a comparison with computational results from the WOPWOP code using measured blade pressures as input is presented.

Description of Experiment

The objective of the test was to experimentally simulate the aerodynamics and acoustics of parallel (2-D), unsteady BVI. The main point of the experiment was to set up a condition that matched, as closely as possible, the simplified model of a rotor blade undergoing an unsteady, parallel interaction with a vortex. Fig. 1 illustrates this simple 2-D BVI model. To provide independent control of the interaction parameters, the vortex was generated separately by a wing tip, placed upstream of the rotor and set at an angle of attack. The rotor was operated at zero thrust to minimize the influence of the rotor's own wake/tip-vortex system. The relative positions of the rotor and wing ensure parallelism of the interaction. Figs. 2 and 3 illustrate the experimental arrangement in the acoustically treated test section of the NASA Ames 80- by 120-Foot Wind Tunnel. Two simi-

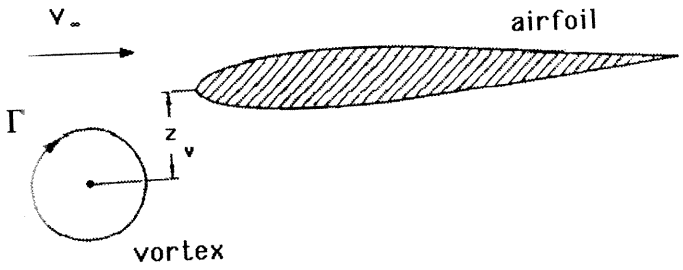

Fig. 1. Analytical model of parallel blade-vortex interaction.

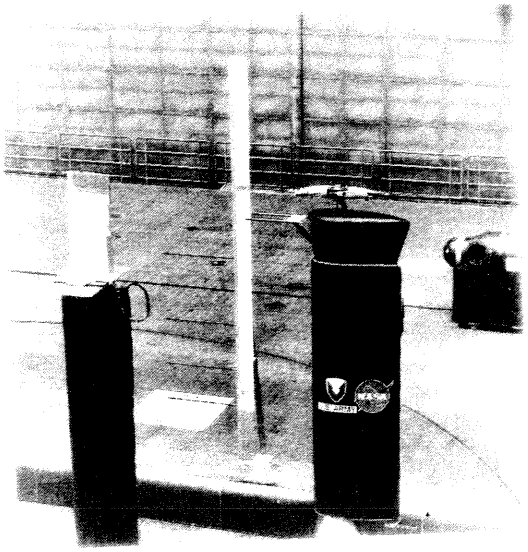

Fig. 2. BVI experiment in the NASA Ames 80- by 120-Foot Wind Tunnel.

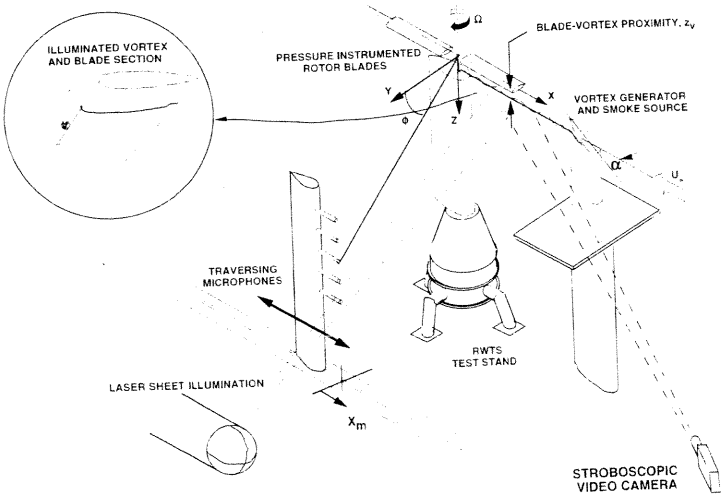

Fig. 3. Sketch of BVI test set-up and definition of parameters.

lar experiments were previously performed by Caradonna (Refs. 6-8); however, that work focused on the aerodynamic aspects of the problem and did not include acoustic measurements because the wind tunnel had acoustically reflective walls. The present experiment extends that work to include acoustic studies.

The major parameters that influence parallel, unsteady BVI are vortex strength and sense (determined by the vortex generator angle of attack, α_v), vortex-blade separation distance (z_v), rotor advance ratio (μ), and hover tip Mach number (M_{tip}). These were all independently controlled.

A small-scale (7-foot diameter), two-bladed, teetering rotor was used. The blades are untwisted and have a rectangular planform with NACA 0012 airfoil sections of 6-inch chord. The blade tip Reynolds number was of the order of 10^6.

The blade surface pressure distribution was measured with a chordwise and spanwise array of 60 absolute pressure transducers (Fig. 4). Two sets of acoustic measurements were made (Figs. 5-6). Two microphones in the near-field of the interaction provided information on the detailed evolution of the acoustic field and can serve to validate "mid-field" calculations of computational aeroacoustics and Kirchhoff methods. A movable array of microphones was used to obtain a limited (due to time constraints) survey of the acoustic far-field.

The characteristics of the vortex were not measured during this experiment, but can be estimated from the work of McAlister and Takahashi on a similarly-generated vortex (Ref. 9), as follows:

$$\Gamma_v = 0.35\, V_\infty\, c_{vg}$$
$$\zeta_v = 0.05\, c_{vg}$$

An extensive set of data for a combination of BVI parameters (Table 1) were obtained. A more detailed description of the experiment and the data acquisition and processing procedures are presented in Ref. 10.

Table 1. Test Matrix

M_{tip}	μ	α_v
0.7	0.2	-12°, +12°, +6°
0.6	0.1	-12°, +12°
	0.15	-12°, +12°
	0.2	-12°, +12°, +6°
0.5	0.2	+12°
0.4	0.2	-12°, +12°
0.25	0.2	-12°, +12°

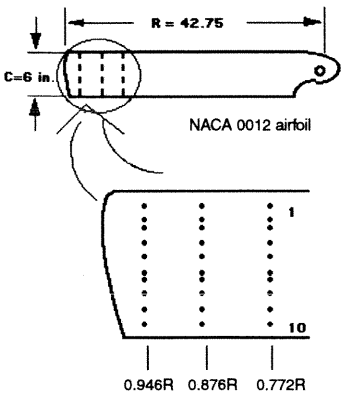

Transducer	Chordwise position
1	0.02
2	0.11
3	0.20
4	0.31
5	0.40
6	0.48
7	0.56
8	0.64
9	0.72
10	0.83

Fig. 4. Blade pressure transducer locations (not to scale). Identical locations for upper and lower surfaces.

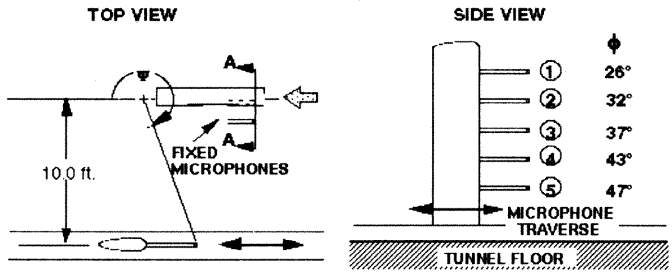

Fig. 5. Far-field microphone positions (not to scale). Elevation angles relative to rotor plane.

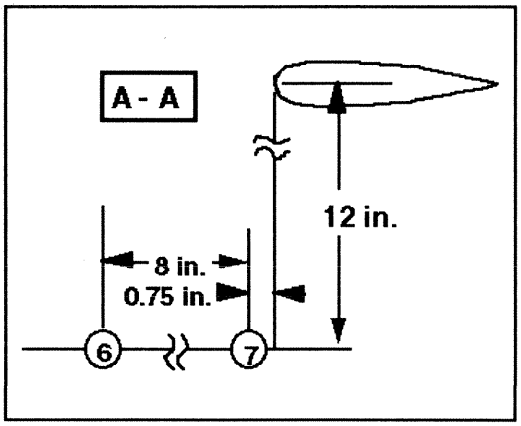

Fig. 6. Near-field microphone positions (not to scale).

Results

This section presents a detailed discussion of the unsteady features of blade pressures during the BVI encounter. The dependence of the acoustic field, as well as the corresponding blade surface pressures, on various parameters of BVI are discussed. Some representative cases of BVI are presented. Finally, some comparisons are presented of experimental acoustic data with computational results from the WOPWOP code using measured blade pressures as input.

Blade pressures

Fig. 7 shows a typical set of pressure-time histories on the upper and lower surfaces of the rotor blade during a nominally head-on (zero miss distance) BVI condition (the vortex generator is set to a position that was

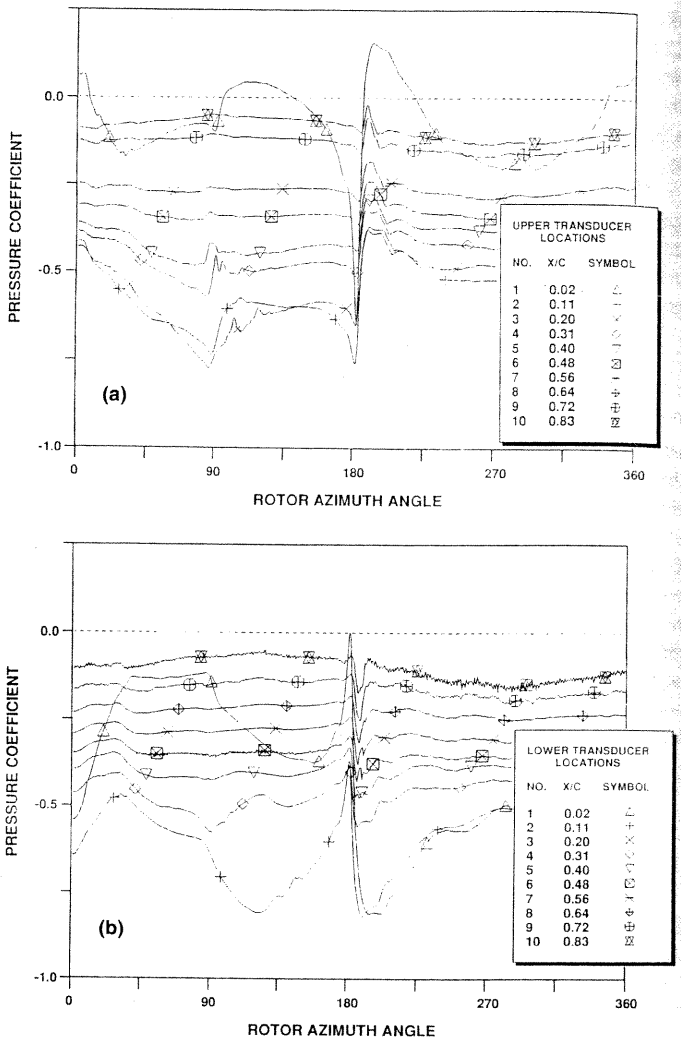

Fig. 7. Blade pressure variations induced by parallel BVI. M_{tip}=0.71, μ=0.2, α_v=+12°, z_v/c=0, r/R=0.88; (a) upper surface, (b) lower surface.

determined in previous flow visualization runs). Data are shown for a full revolution, at 0.876R for a hover tip Mach number of 0.712 and advance ratio of 0.197. The vortex generator was set to an incidence, α_v, of +12°. The flow environment of this rotor is quite dynamic, in spite of the near-zero collective pitch. The upper surface of the rotor blade at the 90° azimuth position exhibits a weak shock, indicative of supercritical flow. Examination of the data at lower Mach numbers (not shown) reveals that the sharp pressure increase disappears, evidence that this is indeed a shock. There is also a weak BVI interaction that occurs near this point (ψ = 90°). Evidently the external vortex is inducing enough blade lift variation for the rotor to have a self generated BVI. However, the most prominent single feature is the parallel BVI event at an azimuth of 180°.

Viewing the pressure-time histories in terms of the events at the leading edge is useful. Fig. 8 shows the time history of the upper and lower surface transducers closest to the leading edge for nominal miss distances of 0.0 and -0.4 chords (0.876R, hover tip Mach number of 0.712, advance ratio of 0.197 and α_v = -12°). The usefulness of the leading edge transducers is that they usually behave similarly to the other transducers — but in a more sensitive manner — and the differential pressure is a good indicator of the lift history. Fig. 8 shows that while the differential pressure is generally not large, except at the BVI, neither is it negligible or particularly smooth. In Fig. 7 we noted the presence of a weak vortex interaction

at 90° azimuth. In Fig. 8 (where the vortex swirl direction is reversed) we see weak vortex interactions at both 90° and 270°. There is considerable reduction in the leading edge pressure variations when the vortex moves from 0.0 to 0.4 chords away from the blade. Note that the primary difference in the BVI occurs at-or-before the point where the sign of the differential pressure reverses. This is the early stage of the BVI where the vortex is near the blade leading edge. The latter stage of the BVI is not greatly affected by the proximity change. These proximity-induced changes are very localized effects as the pressure variations show almost no effect of the vortex movement except near $\psi = 180°$, where the early stages of BVI occurs. Nevertheless, the externally generated vortex does have a global effect on the rotor behavior through its effect on the trim state. The rotor is trimmed to zero flapping in order to consistently locate the blade and vortex with respect to each other. The control inputs required for this trim generate a varying rotor lift together with a wake and the previously noted rotor-wake interactions. The influence of the trim state of the rotor on the details of the BVI time history is not fully understood at present. This is illustrated by noting the effect of reversing the sign of the externally generated vortex. We expect that reversing the sign of the vortex should merely cause the upper and lower surface pressures to reverse places. This does not occur, as indicated by Fig. 9 which shows the upper and lower surface pressure variations corresponding to Fig. 8b, but with a reversal of vortex sign. There are considerable differences between the pressure-time histories between Figs. 9 and 8b. These differences are most prominent at the BVI event, where the magnitude of the early stage differential pressures are greatly reduced, while the latter stage magnitudes are greatly increased. Ref. 11 proposes that this asymmetry of the differential pressure with respect to vortex sign is due to an innate asymmetry of the vortex. This is not unlikely, since the vortex is only 4 chords old at the time of the interaction. In addition, prominent kinks in the leading-edge pressure traces only occur for positive α_v — indicative of the passage of the feeding wake sheet. However, an alternate explanation is that there are rotor collective errors. The important point, however, is that the BVI is a strictly local phenomenon, and can be modeled as such. The effects of collective offset and possible vortex asymmetry can be tested in this modeling process.

The salient details of the BVI are discussed next. Fig. 10 shows the time histories of Fig. 7 on a greatly expanded scale (from about 175° to 210°). Several propagative and convective events are discernible in these data. When the vortex reaches the blade leading edge the upper surface pressures begin an abrupt increase (with the leading edge having the largest pressure variation, this variation decreasing strongly with distance from the leading edge — events with opposite sign occur on the bottom surface). The fact that these particular events occur almost simultaneously from leading to trailing edge is indicative of a very rapid propagative event — downstream from leading to trailing edge — whose propagation speed is the sum of the local speed-of-sound and the local flow velocity. The effect of this first BVI wave appears to be the establishment of a fairly steady pressure level that persists for some duration. The duration of persistence is greatest near the leading-edge and is a nearly linear function of distance from the leading edge. During this persistence interval, several occurrences are seen to move downstream at a slower speed that is of the order of the mean flow velocity. For this particular interaction, this slower event is only seen on the bottom surface. These events are associated with the chordwise passage of the vortex and vortex-generated flow features. (The fact that convective events are not seen equally on both surfaces suggests that the vortex miss distance may not be exactly zero.) These two occurrences were previously noted in the earlier tests that were conducted in the Army 7- by 10-Foot Wind Tunnel (Refs. 6-8). However, the present data also show an additional propagative event not seen in the earlier tests. At about the time the previously mentioned convective events approach the trailing edge a new wave appears — propagating upstream from the trailing edge. This wave has a fairly broad width and moves upstream slowly (at the speed of sound minus the convection speed). This wave probably results from re-establishment of the trailing-edge Kutta condition, either in

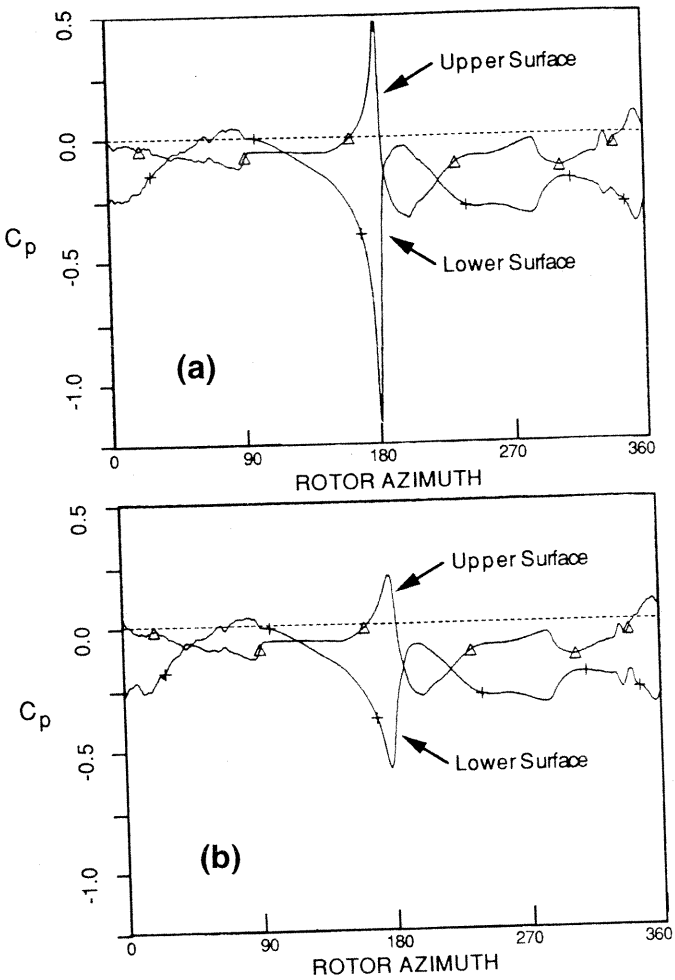

Fig. 8. Leading edge pressure variations induced by parallel BVI. $M_{tip} = 0.71, \mu = 0.2, \alpha_v = -12°$, r/R = 0.88, x/c = 0.02; (a) $z_v/c = 0$, (b) $z_v/c = -0.4$.

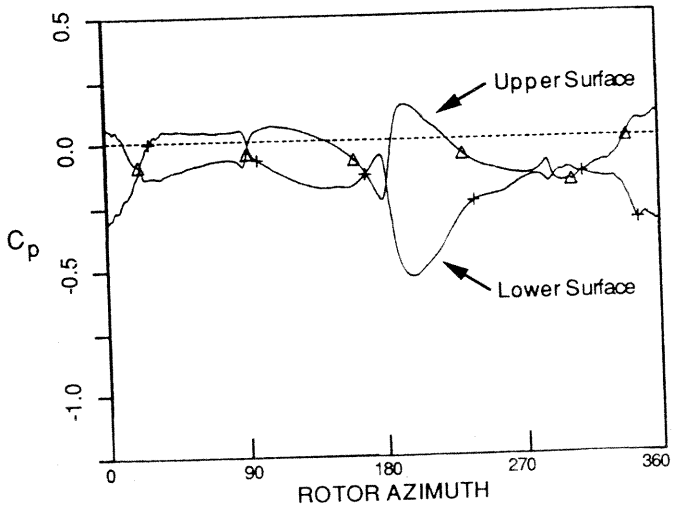

Fig. 9. Leading edge pressure variations induced by parallel BVI. $M_{tip} = 0.71, \mu = 0.2, \alpha_v = +12°$, r/R = 0.88, x/c = 0.02, $z_v/c = -0.4$.

response to the passing vortex or to the original BVI wave, and propagating that information upstream. This secondary or "Kutta wave" occurs at the same time and has opposite sign on the top and bottom surfaces. Because the sign is opposite, we believe that this latter wave is primarily a response to the convective wave rather than to the vortex itself. The inviscid effect of a vortex at a sharp edge is an expansion on both sides. This wave is weak (compared to the initial BVI pulse) and was not seen in previous testing — possibly due to flow unsteadiness. Similar upstream waves emanating from the trailing edge were recently reported by Obermeier and Schurmann (Ref. 12) in high-speed interferometric studies conducted in a shock tube.

The effect of the BVI on the chordwise pressure distribution is shown in Fig. 11 for the same BVI event shown in Fig. 10. Fig. 11a shows the chordwise pressure distribution at an azimuth of about 176°, which is shortly before the impact of the vortex on the leading edge. At this point the lift is still quite small but beginning to rise rapidly. Fig. 11b (ψ = 181°) shows the pressure distribution near the moment of impact of the vortex center on the leading edge. At this point the lift is a maximum and begins to drop rapidly. Fig. 11c (ψ = 184°) shows the pressure distribution only 3 degrees later. At this point the lift is zero and dropping. The lift continues to drop until ψ = 188° (Fig. 11d); the entire shape of the pressure distribution is distorted resulting in a significant differential pressure in the trailing-edge region. This trailing edge loading results in a sharp moment pulse and blade "ringing" that was clearly seen in the root torsion strain gages. This point closely corresponds to the point at which the upstream-moving wave commences. After this point we see the re-establishment of circulatory lift and the differential pressure reduces, as does the total lift. Figs. 11e and 11f show the evolution of the chordwise pressure distribution as the "Kutta wave" propagates upstream. This last point (ψ = 207°) constitutes the termination of the BVI event. We can define the BVI event as that period beginning when the vortex passes the leading edge and ending when the resulting Kutta wave passes the leading edge. These are two easily identifiable events during which time the blade turns about 30 degrees of azimuth, which is about 3 chords of travel at this radial station. The vortex is not close to the blade in the latter stages of the interaction, and this explains the previously-noted lack of sensitivity of these phases of the interaction to miss-distance.

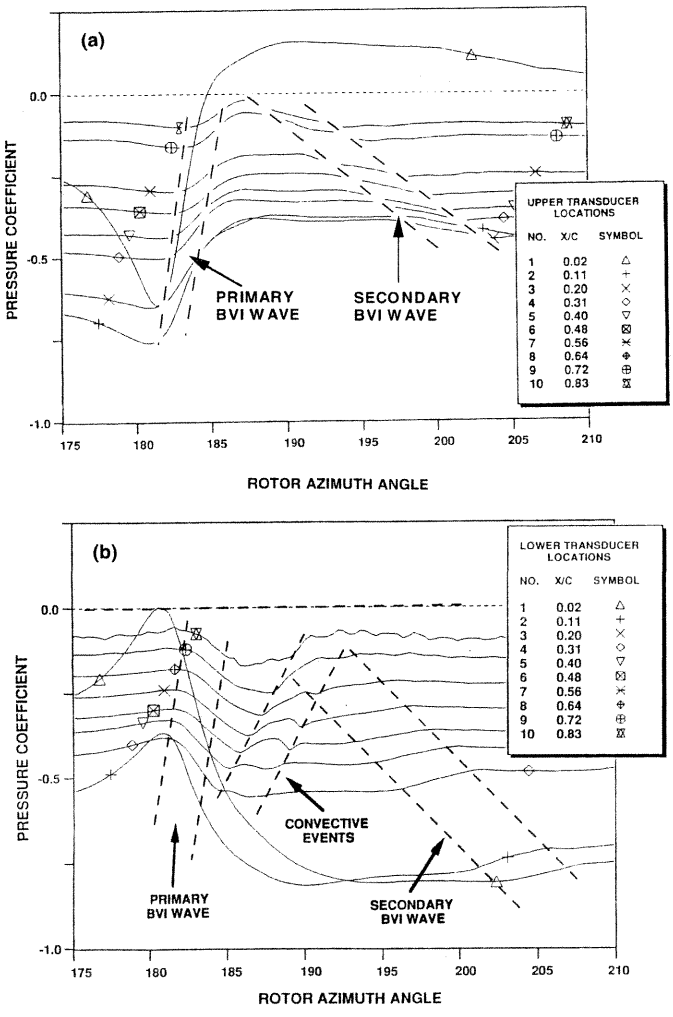

Fig. 10. Blade pressure variations induced by parallel BVI. Expanded azimuth scale. M_{tip} = 0.71, μ = 0.2, α_v = +12°, r/R = 0.88, z_v/c = 0; (a) upper surface, (b) lower surface.

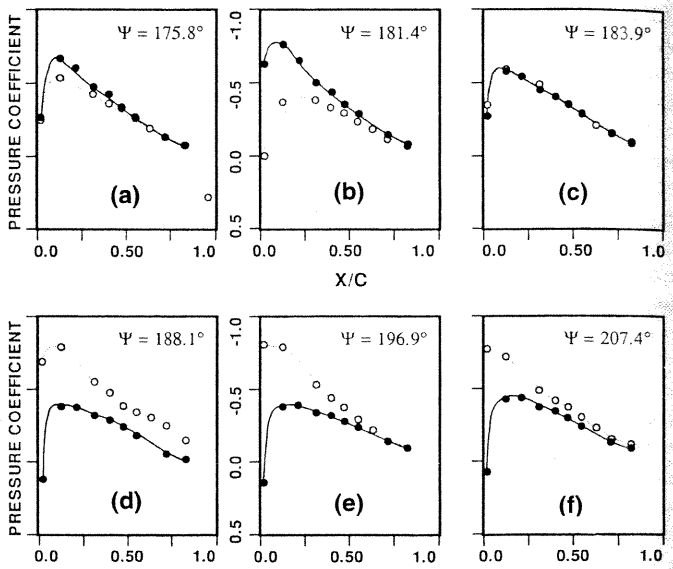

Fig. 11. The effect of parallel BVI on the rotor chordwise pressure distribution. M_{tip} = 0.71, μ = 0.2, α_v = +12°, r/R = 0.88, z_v/c = 0; (•) upper surface, (○) lower surface.

The most prominent feature of the BVI event is the rapid pressure jump which occurs at the leading edge. Since the pressure varies from a distinct peak (which occurs when the vortex is at the leading edge) to a subsequent well-defined "plateau," the magnitude of this change (shown in Fig. 12 for the bottom surface and for several vortex generator angles-of-attack) provides a convenient characterization of the BVI strength. We have summed the absolute values of these pressure coefficient jumps for the upper and lower surfaces, here termed the "BVI Pressure Jump" or χ_{bvi}, as a simple measure of the BVI. Fig. 13 plots χ_{bvi} as a function of nominal vortex miss distance for vortices of opposite sign. For a vortex generator incidence angle of +12°, χ_{bvi} peaks at a miss distance of about 0.125c, in contrast to the α_v=-12° case which peaks at a miss distance of z_v=0 chord.

Fig. 14 is the acoustic field measured by one of the far-field microphones corresponding to the blade pressures of Fig. 7, and is typical of the BVI acoustic data obtained during the test. As indicated on the figure, the change in acoustic pressure from the peak of the initial rise to the minimum peak is a convenient measure of the BVI acoustic event, which is herein referred to as the "BVI acoustic amplitude, Π_{bvi}." Π_{bvi} is plotted as a function of nominal vortex miss distance in Fig. 15. Consistent with Fig. 13 for blade pressures, for a vortex generator incidence angle of +12°, Π_{bvi} appears to peak at a miss distance of approximately 0.125c, in contrast to

the α_v=-12° case which peaks at a miss distance of z_v=0 chord.

These observations suggest that the nominal vortex location (α_v = +12°) is probably in error by about 0.1c (for unknown reasons that could include errors in the vortex generator position gage or the blade flap gage). For a vortex generator setting of -12° there was no apparent anomaly in the vortex location readout. In addition, the maximum χ_{bvi} for α_v = -12° is greater than that for α_v = +12° (by about 10%). Similarly, the maximum Π_{bvi} for α_v = -12° is greater than that for α_v = +12° (by about 25%). The microphones show much greater sensitivity to vortex swirl direction than the leading edge surface pressures.

These observations probably indicate that the magnitude of the lift of the vortex generator — and hence of the vortex strength — is not the same for the two different incidence angle settings. However, the proximity trend is very similar for the opposite vortex swirl cases. This indicates that, while there may indeed be some asymmetry of the vortex or a blade pitch angle offset, there is an essential symmetry to the interaction. The ability to accurately predict the detailed features of the blade pressures during BVI presents a challenge to the analysts.

Acoustics

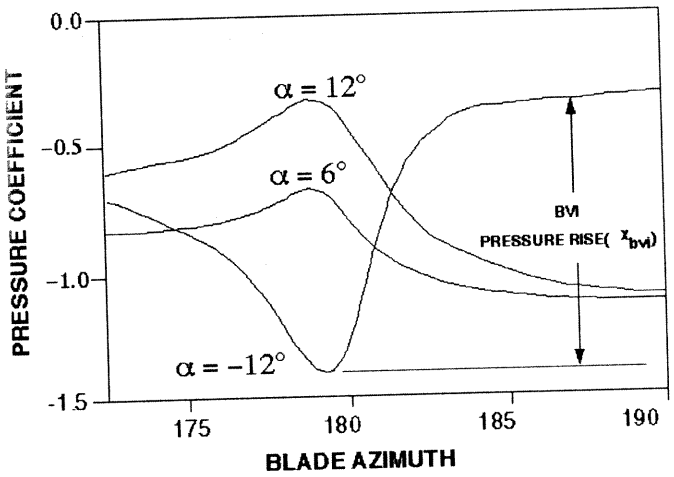

Fig. 12. The effect of vortex strength and sense on BVI lower surface pressure variations. M_{tip} = 0.71, μ = 0.2, r/R = 0.88, x/c = 0.02, z_v/c=0.

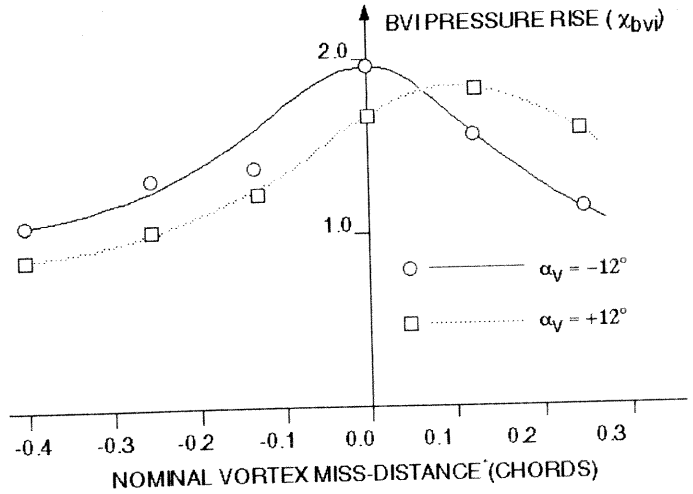

Fig. 13. The effect of vortex proximity on the BVI pressure rise. M_{tip} = 0.71, μ = 0.2.

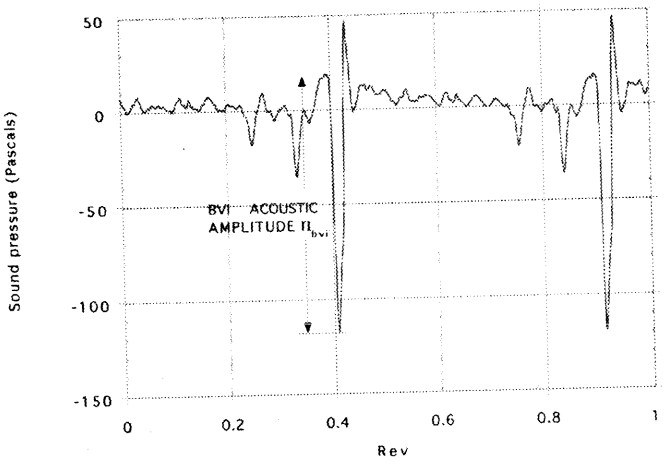

Fig. 14. Typical far-field acoustic time history for parallel BVI.

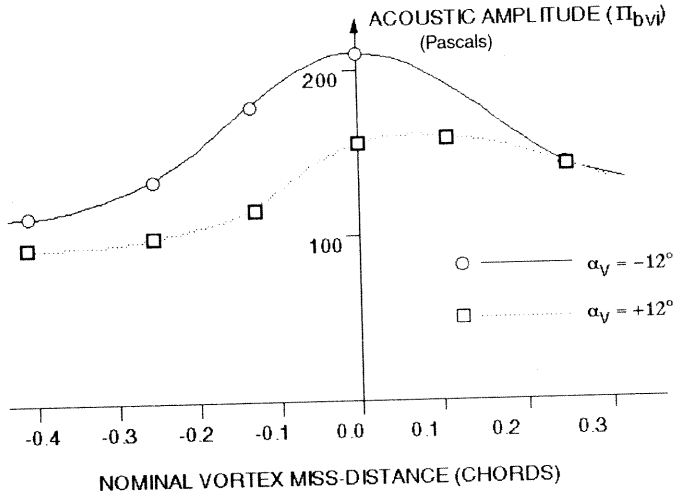

Fig. 15. The effect of vortex proximity on the BVI acoustic amplitude. M_{tip} = 0.71, μ = 0.2.

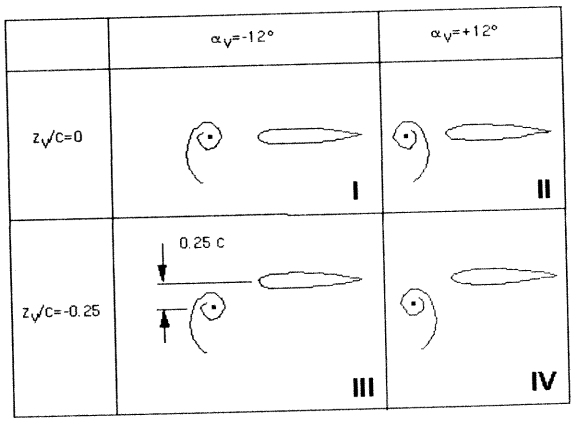

Fig. 16. Four BVI configurations.

Far-field and near-field acoustic data are presented and discussed for four representative cases of BVI for which the tip Mach number and advance ratio are fixed at M_{tip}=0.712 and μ=0.196, respectively. The four cases are for interaction occurring with vortices of opposite sense (swirl direction), obtained by setting the vortex generator wing at +12° and -12° angle of incidence, and for head-on interaction with the vortex, as well as with the vortex 0.25 blade chord below the blade. These four cases are il-

lustrated in Fig. 16. Case III corresponds to the usual advancing side BVI.

Fig. 17 shows the acoustic pressure measured by far-field microphones 2 -5 (Fig. 5) for the four cases of Fig. 16. These data were obtained with the microphone traverse positioned at 90° relative to the rotor hub (i.e. directly to the retreating side of the hub). Immediately noticeable is the relative phasing of the pulses due to the differences in source-to-microphone distances. Several secondary pulses, which we attribute to tunnel floor reflections (Ref. 10) are also evident. There is a reversal in the sign of the acoustic pressure pulse corresponding to the reversal in the swirl direction of the vortex. No major directivity changes are evident over the range of elevation angles spanned by these microphones. Geometry limitations did not allow positioning microphones at larger elevation angles to better corroborate acoustic field directivity.

There is a noticeable change in the shape of the BVI pulses between head-on interaction and when the vortex is below the blade. The pulse shapes for the head-on cases (Cases I and II) display a sharper rise to a higher peak which is followed by an equally sharp drop. Prior to reaching ambient level, however, the pulse abruptly widens. The z_v=-0.25-chord cases (Cases III and IV), on the other hand, display a more symmetric pulse shape with a more gradual rise than for head-on impact.

As expected, the acoustic pulse amplitudes are much larger for the direct impact cases (Cases I and II) than when the vortex is below the blade (Cases III and IV). In addition, for head-on interaction, the pulse amplitude for the α_v=-12° case (Case I) is significantly larger than the α_v=+12° case (Case II). This is not the case when the vortex is below the blade.

Fig. 18 shows the corresponding near-field microphone (Fig. 6) data for the four cases of Fig. 16. Microphone 7 was closer to the blade, at the 180° azimuth position, but at a larger directivity angle than microphone 6. Fig. 18 exhibits several interesting features.

The first feature to note is the change in pulse shape with vortex swirl direction. The α_v=+12° cases (Cases II and IV) contain a low amplitude feature at the leading edge reminiscent of thickness noise. This is not seen in the α_v=-12° cases (Cases I and III), most likely because, while the BVI pulse has reversed in amplitude with a reversal in vortex swirl, the thickness noise remains unchanged. Their superposition results in the observed pulse shapes. This is more pronounced for microphone 7 than for microphone 6, most likely because of the directionality of this mechanism. The presence of this feature may be the result of the specific operating state of the rotor near the 180° azimuth position.

Another interesting feature to note is the relative amplitudes of the two near-field microphones. Whereas for α_v=-12° (Cases I and III) the amplitude for microphone 6 is the same or smaller than that for microphone 7, as would be expected since microphone 6 is at a greater distance, for α_v=+12° (Cases II and IV) microphone 6 exhibits a larger acoustic pulse amplitude. There is also a noticeable difference in the pulsewidths for the two microphones in all cases. These are most likely the result of the complex wave components and their interactions in the near-field.

Computations

Several papers have been published (Refs. 13 and 14) comparing computations of both near- and far-field acoustics of parallel BVI to these ex-

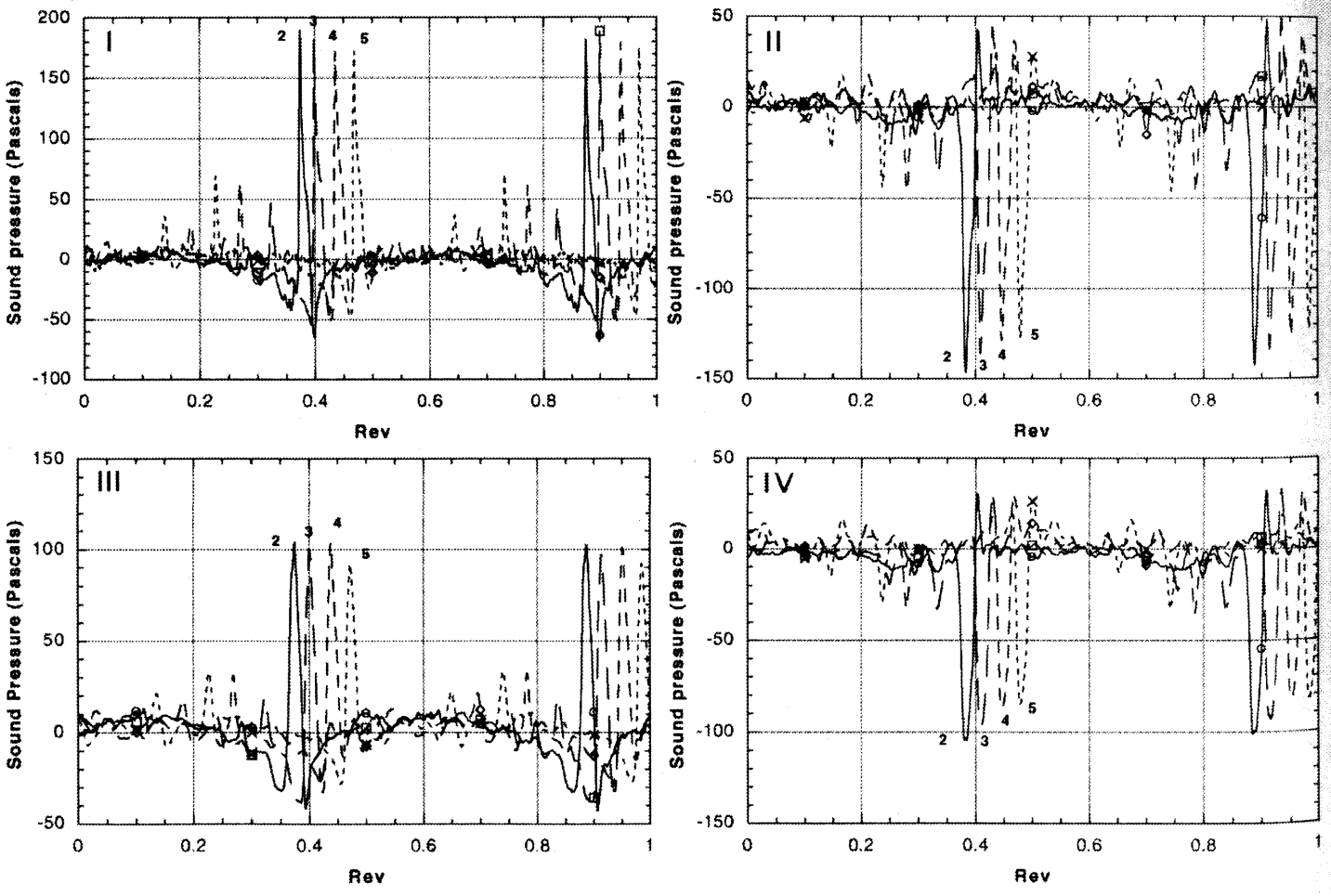

Fig. 17. Far-field acoustic pressures for the four BVI configurations of Fig. 16. Microphone numbers are indicated on the figure. M_{tip}=0.71, μ=0.2.

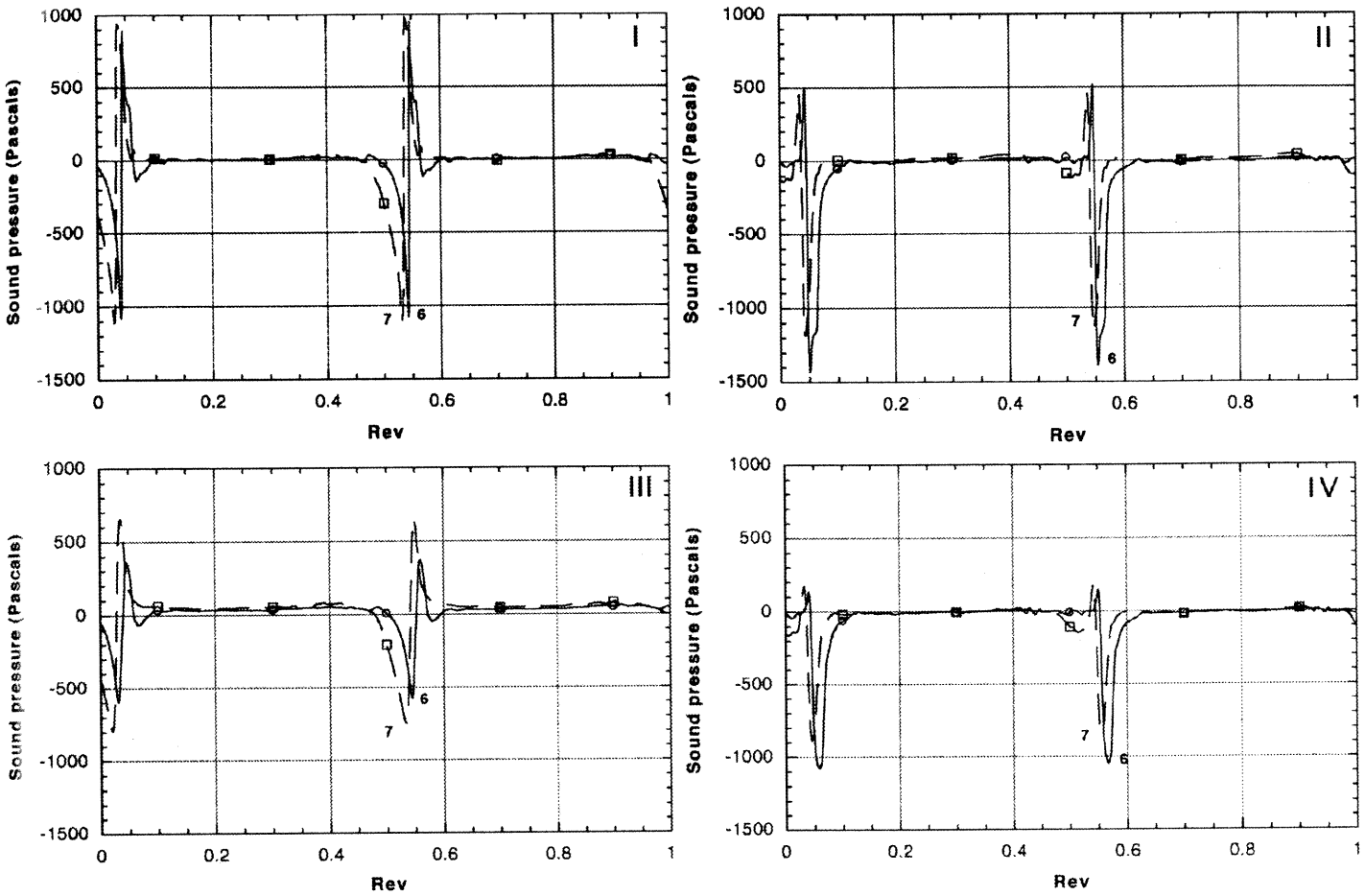

Fig. 18. Near-field acoustic pressures for the four BVI configurations of Fig. 16. Microphone numbers are indicated on the figure. $M_{tip} = 0.71, \mu = 0.2$.

perimental data. These have been "first principles" approaches, not utilizing the measured blade surface pressures, and have obtained encouraging results.

We present results of a computational study of BVI acoustics using measured blade pressures. Acoustic predictions were made using the rotor acoustic prediction code WOPWOP for configuration III of Fig. 16 (M_{tip}=0.7, μ=0.2, α_v=-12°, vortex 0.25 blade chord below rotor). Measured blade pressures obtained at three radial stations were used as input and acoustic predictions were made for four far-field microphones and two near-field microphones.

The WOPWOP code is based on the acoustic formulation 1A of Farassat (Ref. 2). This formulation is a time-domain representation of the Ffowcs Williams-Hawkings equation, excluding the volume source or "quadrupole" term. Since high speed impulsive noise is substantially shock-formation related, it is not accounted for in the formulation. Neither are volume source effects of transonic BVI. Formulation 1A was developed to predict discrete frequency noise of helicopter rotors, and is valid for arbitrary blade motion, geometry and observer location. The WOPWOP code predicts thickness and loading noise at a specified observer location. These noise sources are blade surface terms.

For the acoustic predictions, the blade pressures measured at the three radial stations, r/R = 0.772, 0.876, and 0.946 were used as input. The computational grid was adjusted in the radial direction to locate the panel centers at the blade pressure measurement locations. The number of panels was varied between 10 and 50 radially between 0.75R and the tip to check for numerical differences that may occur due to grid size. No difference in the predicted acoustics for the far-field microphones was seen. The chordwise computation grid was also varied, from 27 chordwise locations to 47. Again, no difference in the predicted acoustics for the far-field microphones was seen. Finally, the number of time steps used in the computation was varied from 256 to 512 time steps per blade passage. The maximum level of the BVI peak for all the acoustic time histories increased by less than 3%, and the computation time approximately doubled. Thus 256 time steps per blade passage was chosen for the remainder of the predictions. Linear interpolation of the measured data onto the computation grid was used for the chordwise, radial and azimuthal (time) directions.

Predicted and measured acoustic time histories for the four far-field and two near-field microphones are shown in Figs. 19 and 20, respectively. The predictions were made with 50 radial panels between 0.75R and the tip, 27 chordwise panels from leading to trailing edge and 256 time steps per blade passage. In the figures the prediction is shown with circles and the measured data is shown as a solid line. For each of the far-field microphones the predicted maximum peak levels are slightly lower than the measured. However the comparison of the predicted pulse width with the measured pulse width is in good agreement. The predictions for the near-field microphone 6 (Fig. 20) overpredicts both the positive and negative peak slightly. However the predicted pulse width and character is in very good agreement with the measurement. For the near-field microphone 7, the negative peak is underpredicted by approximately 100 pa, but the overall predicted pulse width and character is in very good agreement with the measurement.

Since the measured data were obtained for parallel interaction, the vor-

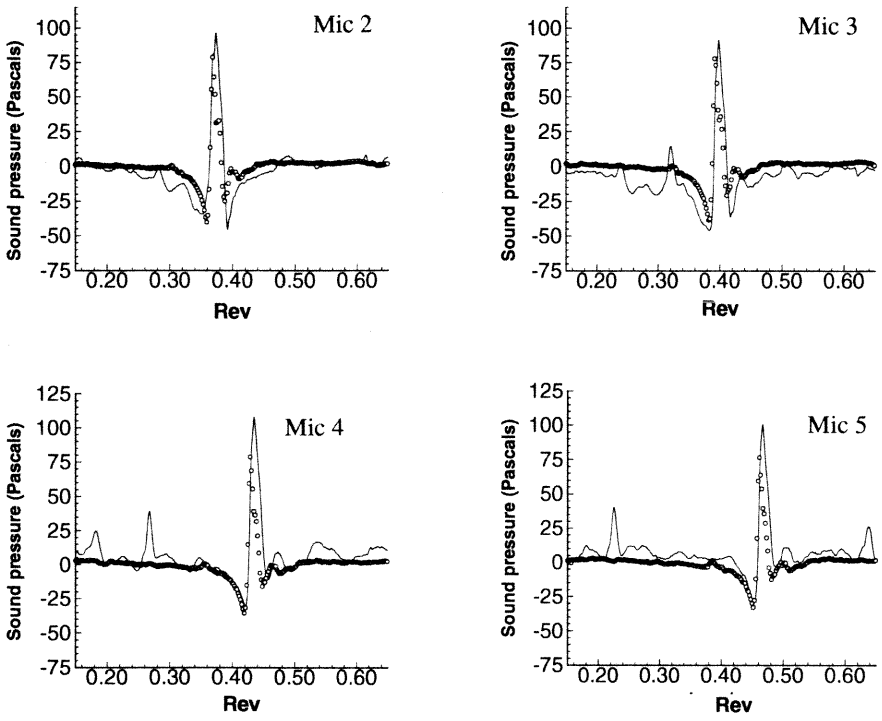

Fig. 19. WOPWOP predictions: far-field microphones. Sources distributed 0.75R to tip. $M_{tip} = 0.71, \mu = 0.2, \alpha_v = -12°, z_v/c = -0.25$; (○) predicted, (———) measured.

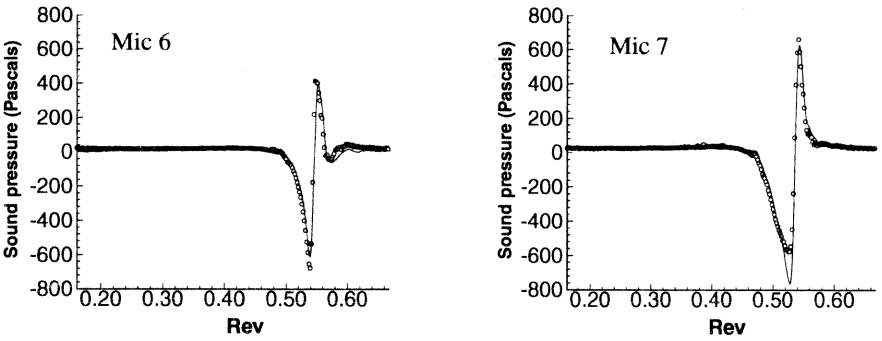

Fig. 20. WOPWOP predictions: near-field microphones. Sources distributed 0.75R to tip. $M_{tip} = 0.71, \mu = 0.2, \alpha_v = -12°, z_v/c = -0.25$; (○) predicted, (———) measured.

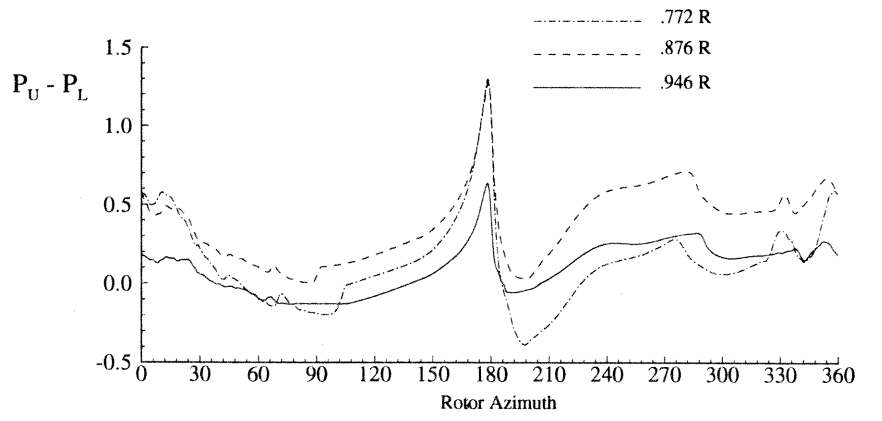

Fig. 21. Measured blade pressures at three radial stations. $M_{tip} = 0.71, \mu = 0.2, \alpha_v = -12°, z_v/c = -0.25$.

tex was in close proximity to the blade for the full blade span. The measured blade pressures used for the acoustic predictions in Figs. 19 and 20 included only the outer 25% of the blade. Thus the noise source panels on the inner part of the blade are not considered in the predicted acoustics. This may explain the underprediction of the peak amplitudes. The measured peak to peak pressures at r/R=0.876 and 0.772 are nearly the same, as shown in Fig. 21. From this, the assumption is made that the measured pressures at r/R=0.772 could be extrapolated in WOPWOP for inboard pressures to, say, r/R=0.5. Acoustic predictions made with these added inboard sections are shown in Figs. 22 and 23. Of course this is an overestimation, since the velocity inboard is decreasing and the pressures due to the vortex interaction will be less, assuming this is a truly parallel interaction. The maximum peak in the acoustic predictions compare very well with the measurements for the far-field microphones as shown in Fig. 22. However, the prediction at the near-field microphone 6 (Fig. 23) overpredicts the negative pulse even more. The prediction at microphone 7 agrees quite well with the measured data.

As a final test, the measured pressures at r/R=0.772 were extrapolated to inboard station r/R=0.3. As mentioned earlier, this will result in an overestimation of the peak acoustic amplitudes. However, it should result in a more accurate prediction of the acoustic waveform if the inputs are truly from parallel BVI. As expected the predictions overpredicted all the peaks for all microphones, but the predicted waveforms better matched the width and overall shape of the measured data. This study indicates that good agreement between measured and predicted acoustic time signatures for parallel BVI may be obtained using measured pressures at three outboard radial locations. However, to obtain the most accurate predictions, blade pressures over most of the blade span (in this example, at least 50%) should be used.

Summary

This paper presented the results from an experimental study of parallel Blade-Vortex Interaction. A nominally non-lifting rotor was operated in close proximity to the tip-vortex generated by an upstream wing — thus simulating a very simple parallel BVI. Simultaneous rotor blade surface pressure and near- and far-field acoustic data were obtained for a range of vortex miss distances, rotor speeds and vortex strengths. The rotor, though nominally non-lifting, actually generates a non-negligible wake of its own and the behavior of this wake, in response to the external vortex, is not simple or well understood. Many detailed features in both the blade pressure and acoustic data were identified and discussed. These include the presence of a downstream, and a much weaker upstream, wave on the blade surface. However, the primary BVI event is prominent and quite localized with no obvious coupling to other rotor events. It is possible to define simple interaction parameters (both in the surface pressures and acoustic signals) that characterize the BVI and give well-defined trends for the BVI behavior as a function of operational quantities, especially the miss-distance. These parameters indicate and provide a

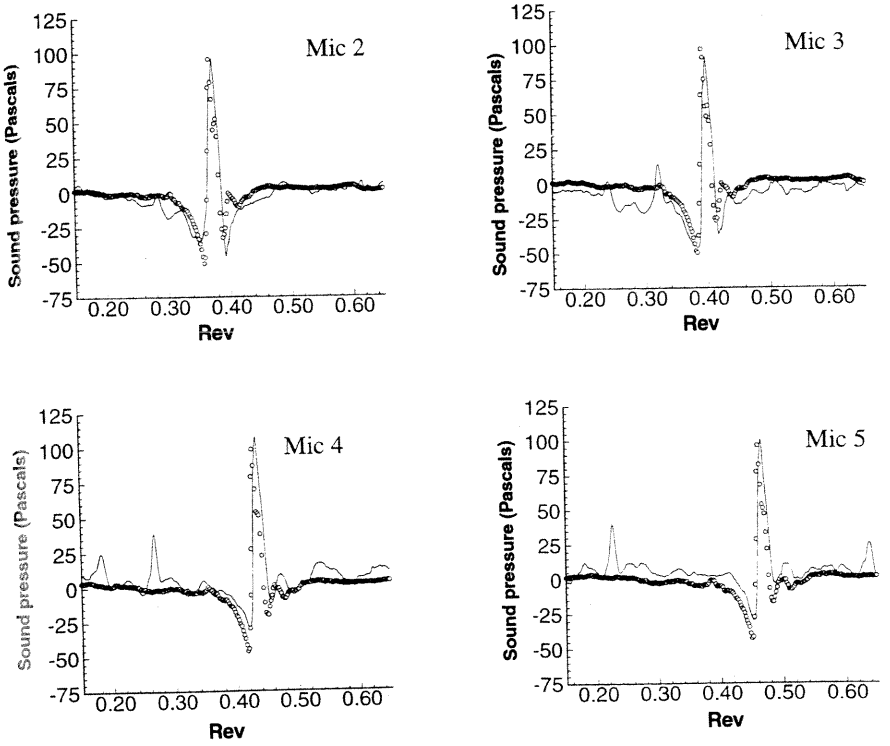

Fig. 22. WOPWOP predictions: far-field microphones. Sources distributed 0.5R to tip. $M_{tip} = 0.71, \mu = 0.2, \alpha_v = -12°, z_v/c = -0.25$; (◦) predicted, (———) measured.

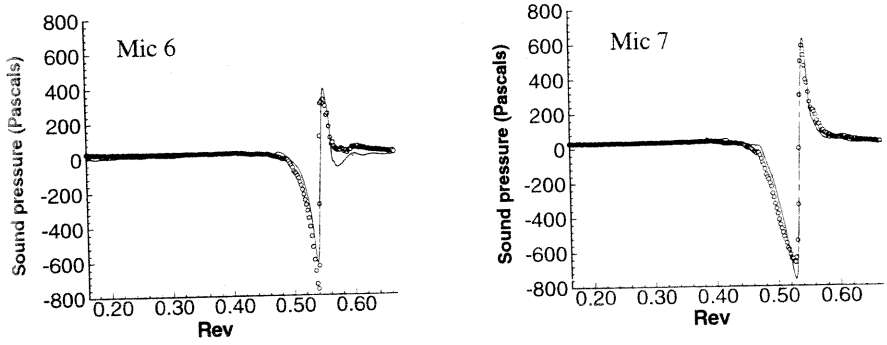

Fig. 23. WOPWOP predictions: near-field microphones. Sources distributed 0.5R to tip. $M_{tip}=0.71, \mu=0.2, \alpha_v=-12°, z_v/c=-0.25$; (◦) predicted, (———) measured.

measure of possible miss-distance errors, thus guiding the choices of geometry variations that will have to be made in future computations. Study of the leading-edge surface pressure variations indicates a prominent load asymmetry behavior with respect to vortex sign. There is a corresponding asymmetry in the resulting acoustic field. There are several potential explanations of this asymmetry, of which the simplest is the possible presence of a blade pitch angle offset. Future computations may require some variation in the blade incidence in order to better define the effects of such an offset. In spite of such recognized complications, the test reveals detailed features of the BVI, the computational duplication of which will provide a definitive verification of our understanding of BVI-induced loading and acoustics.

A comparison was made between one of the experimental cases and computations from the WOPWOP acoustic prediction code using measured blade pressures for input. The code yielded good results in both the far-field and the near-field. Pulsewidths were computed quite well. The peak-to-peak amplitudes were predicted to within approximately 15% or better in most cases.

Acknowledgments

The authors wish to acknowledge the assistance of Dr. Judy Gallman and Ms. Megan McCluer in the analysis and interpretation of the experimental results.

References

[1]George, A.R. and Chang, S.B., "Noise Due to Transonic Blade-Vortex Interactions," American Helicopter Society 39th Annual Forum, St. Louis, MO, May 1983.

[2]Brentner, K.S., "Prediction of Helicopter Rotor Discrete Frequency Noise," NASA TM 87721, Oct 1986.

[3]Gallman, J.M., "The Validation and Application of a Rotor Acoustic Prediction Computer Program," Army Science Conference, Durham, NC, Jun 1990.

[4]Xue, Y. and Lyrintzis, A.S., "The Use of a Rotating Kirchhoff Formulation for 3-D Transonic BVI Far-Field Noise," American Helicopter Society 49th Annual Forum, St. Louis, MO, May 1993.

[5]Baeder, J.D., "The Computation and Analysis of Acoustic Waves In Transonic Airfoil-Vortex Interactions," Ph. D. Thesis, Stanford University, Sep 1989.

[6]Caradonna, F.X., Laub, G.H., and Tung, C., "An Experimental Investigation of the Parallel Blade-Vortex Interaction," 10th European Rotorcraft Forum, The Hague, Netherlands, Sep 1984.

[7]Caradonna, F.X., Lautenschlager, J.L., and Silva, M.J., "An Experimental Study of Rotor-Vortex Interactions," AIAA Paper No. 88-0045, AIAA 26th Aerospace Sciences Meeting, Reno, NV, Jan 1988.

[8]Caradonna, F.X., Strawn, R.C., Bridgeman, J.O., "An Experimental and Computational Study of Rotor-Vortex Interactions," 14th European Rotorcraft Forum, Milano, Italy, Sep 1988.

[9]McAlister, K.W. and Takahashi, R.K., "NACA 0015 Wing Pressure and Trailing Vortex Measurements," NASA TP 3151, Nov 1991.

[10]Kitaplioglu, C. and Caradonna, F.X., "Aerodynamics and Acoustics of Blade-Vortex Interaction Using an Independently Generated Vortex," American Helicopter Society Aeromechanics Specialists Conference, San Francisco, CA, Jan 1994.

[11]Bridgeman, J.O., Ramachandran, K., Caradonna, F.X., and Prichard, D., "The Application of Vorticity Embedding to Parallel Blade-Vortex Interactions," AIAA Paper No. 94-1919, 12th AIAA Applied Aerodynamics Conference, Colorado Springs, CO, Jun 1994.

[12]Obermeier, F. and Schurman, O., "Experimental Investigation on 2D Blade-Vortex-Interaction Noise," AIAA Paper No. 93-4334, 15th AIAA Aeroacoustics Conference, Long Beach, CA, Oct 1993.

[13]Strawn, C.S., Biswas, R., and Lyrintzis, A.S., "Helicopter Noise Predictions Using Kirchhoff Methods," American Helicopter Society 51st Annual Forum, Fort Worth, TX, May 1995.

[14]McCluer, M.S., Baeder, J.D., and Kitaplioglu, C., "Comparison of Experimental Blade-Vortex Interaction Noise With Computational Fluid Dynamic Calculations," American Helicopter Society 51st Annual Forum, Fort Worth, TX, May 1995.